Atmos. Chem. Phys. Discuss., 14, 19357–19394, 2014
www.atmos-chem-phys-discuss.net/14/19357/2014/
doi:10.5194/acpd-14-19357-2014

Atmospheric Chemistry and Physics Discussions

Tropospheric vertical column densities of NO_2 over managed dryland ecosystems (Xinjiang, China): MAX-DOAS measurements vs. 3-D dispersion model simulations based on laboratory derived NO emission from soil samples

B. Mamtimin[1], T. Behrendt[1], M. M. Badawy[1,2], T. Wagner[3], Y. Qi[1,4], Z. Wu[1,5], and F. X. Meixner[1]

[1]Biogeochemistry Department, Max Planck Institute for Chemistry, Mainz, Germany
[2]Department of Geography, Faculty of Arts, Ain-Shams University, Egypt
[3]Air Chemistry Department, Max Planck Institute for Chemistry, Mainz, Germany
[4]International Cooperation Department, National Center for Climate Change Strategy and International Cooperation, Beijing, China
[5]Institute of Geography Science, Xinjiang Normal University, China

Received: 16 April 2014 – Accepted: 13 July 2014 – Published: 28 July 2014

Correspondence to: B. Mamtimin (buhalqem.mamtimin@mpic.de)

Published by Copernicus Publications on behalf of the European Geosciences Union.

ACPD
14, 19357–19394, 2014

Abstract

We report on MAX-DOAS observations of NO_2 over an oasis-ecotone-desert ecosystem in NW-China. There, local ambient NO_2 concentrations originate from enhanced biogenic NO emission of intensively managed soils. Our target oasis "Milan" is located at the southern edge of the Taklimakan desert, very remote and well isolated from other potential anthropogenic and biogenic NO_x sources. Four observation sites for MAX-DOAS measurements were selected, at the oasis center, downwind and upwind of the oasis, and in the desert. Biogenic NO emissions in terms of (i) soil moisture and (ii) soil temperature of Milan oasis' (iii) different land-cover type sub-units (cotton, Jujube trees, cotton/Jujube mixture, desert) were quantified by laboratory incubation of corresponding soil samples. Net potential NO fluxes were up-scaled to oasis scale by areal distribution and classification of land-cover types derived from satellite images using GIS techniques. A Lagrangian dispersion model (LASAT, Lagrangian Simulation of Aerosol-Transport) was used to calculate the dispersion of soil emitted NO into the atmospheric boundary layer over Milan oasis. Three dimensional NO concentrations (30 m horizontal resolution) have been converted to 3-D NO_2 concentrations, assuming photostationary state conditions. NO_2 column densities were simulated by suitable vertical integration of modeled 3-D NO_2 concentrations at those downwind and upwind locations, where the MAX-DOAS measurements were performed. Downwind-upwind differences (a direct measure of Milan oasis' contribution to the areal increase of ambient NO_2 concentration) of measured and simulated slant (as well as vertical) NO_2 column densities show excellent agreement. This agreement is considered as the first successful attempt to prove the validity of the chosen approach to up-scale laboratory derived biogenic NO fluxes to ecosystem field conditions, i.e. from the spatial scale of a soil sample (cm^2) to the size of an entire agricultural ecosystem (km^2).

ACPD
14, 19357–19394, 2014

1 Introduction

Emissions of nitric oxide (NO) are important in regulating chemical processes of the atmosphere (Crutzen, 1987). Once emitted into the atmosphere, NO reacts rapidly with ozone (O_3) to nitrogen dioxide (NO_2) which, under daylight conditions, is photolyzed back to NO ($\lambda \leq 420$ nm). For that reason, NO and NO_2 are usually considered as NO_x ($NO_x = NO + NO_2$). Ambient NO_x is a key catalyst in atmospheric chemistry: during the atmospheric oxidation of hydrocarbons its ambient concentration determines whether ozone (O_3) is photochemically generated or destroyed in the troposphere (Chameides et al., 1992). While the combustion of fossil fuels (power plants, vehicles) is still the most important global NO_x source (approx. 25 Tg a^{-1} in terms of mass of N), biogenic NO emissions from soils have been estimated to range between 6.6 and 9.6 Tg a^{-1} (Denman et al., 2007). The considerable uncertainty about the range of soil biogenic NO emissions stems from widely differing estimates of the NO emission. Moreover, the uncertainties in the NO emission data from semi-arid, arid, and hyper-arid regions are very large (mainly due to a very small number of measurements being available). These ecosystems, however, are considered to contribute more than half to the global soil NO source (Davidson and Kingerlee, 1997), and make approx. 40 % of planet Earth's total land surface (Harrison and Pearce, 2000).

Production (and consumption) of NO in the soil depends mainly on soil microbial activity and is mainly controlled by soil temperature, soil moisture, and soil nutrient concentration (Conrad, 1996; Meixner and Yang, 2006; Ludwig et al., 2001). Any natural or anthropogenic action that result in the inputs of nutrients (e.g. by fertilizer application) and/or modification of soil nutrient turnover rates has a substantial effect on soil biogenic NO emission. The rapid (economically driven) intensification of arid agriculture (oasis agriculture), particularly by enlargement of the arable area and by enhancement of necessary irrigation leads inevitably to the increase of soil biogenic NO emissions. Since those microbial processes which underlay NO production and NO consumption in soils are confined to the uppermost soil layers (< 0.05 m depth, Rudolph et al., 1996),

ACPD
14, 19357–19394, 2014

the most direct method for their characterization and quantification is usually realized by laboratory incubation of soil samples; corresponding measurements result in the determination of so-called net potential NO fluxes, which are explicit functions of soil moisture, soil temperature, and ambient NO concentration (Behrendt et al., 2014).

Tropospheric NO_2 column densities can be retrieved from satellite observations using differential optical absorption spectroscopy (DOAS) (e.g. Leue et al., 2001; Richter and Burrows, 2002; Beirle et al., 2004). Identification and quantification of the sources of tropospheric NO_2 column densities are important for monitoring air quality, for understanding radiative forcing and its impact on local climate. Ground-based Multi Axis Differential Optical Absorption Spectroscopy (MAX-DOAS) is a novel measurement technique (Hönninger et al., 2004) that represents a significant advantage over the well-established zenith scattered sunlight DOAS instruments, which are mainly sensitive to stratospheric absorbers. From NO_2 slant column densities, retrieved from measurements at different elevation angles, information about tropospheric NO_2 profiles and/or tropospheric vertical column densities can be obtained (Sinreich et al., 2005; Wittrock et al., 2004; Wagner et al., 2011).

In this paper we concentrate (a) on ground-based MAX-DOAS measurements of slant and vertical NO_2 column densities over an intensively used oasis of the Taklimakan desert (NW-China), (b) on biogenic NO emissions derived from laboratory incubation measurements on oasis soil samples, (c) on up-scaling of the laboratory results to the oasis level, (d) calculation of atmospheric boundary layer NO_2 concentrations by suitable NO $\rightarrow$ NO_2 conversion and 3 dimensional dispersion modelling, and (e) on simulating slant and vertical NO_2 column densities from the calculated 3-D-NO_2 distributions by integration along the MAX-DOAS light path. The final aim is comparison and discussion of the results obtained under (a) and (e).

ACPD
14, 19357–19394, 2014

2 Materials and methods

2.1 Research area

After two "searching field campaigns" (2008 and 2009) in the Xinjiang Uighur Autonomous Region of NW-China, the oasis "Milan" has been identified as the target oasis for the presented research. The contemporary oasis Milan, identical to the ancient silk-road post "Miran", belongs to the county "Ruoqiang" of the Xinjiang province and is located in the southern Taklimakan Desert on the foot of the Altun Shan Mountains (39.25° N, 88.92° E, 998 m a.s.l.). In the early 1950s, the delta-shaped oasis (see Fig. 1) has been established as an agricultural co-operative "state farm" (*Xinjiang Production and Construction Crop*) and covers nowadays about 100 km^2. Milan oasis can be geomorphologically classified as a "mountain-oasis-ecotone-desert system (MOED system)" consisting of Gobi (gravel) desert, a salty transition zone surrounding the oasis, and dryland farming with irrigation. The latter consists only of two crops, cotton and jujube trees (*Ziziphus Jujuba* L., "red date"), which are planted, irrigated, and fertilized following standardized protocols and growing on rectangular fields (approx. 10 ha) of pure cultures or mixtures of it. The general energy supply of Milan oasis is entirely provided by nearby hydropower plants, and battery powered trikes dominate the local public and private transport. Consequently, anthropogenic NO_x emissions of Milan oasis are considered as very low, if not negligible. Beyond that, Milan oasis is isolated by the desert from neighbouring oases by 80 to 400 km. Therefore, the dominant NO_x source of Milan oasis are biogenic NO emissions from its intensively managed crop fields; the oasis can be undoubtedly considered as a large "hotspot in the middle of nothing". Given this very specific situation, it is certainly justified to assume that (a) NO_2 concentrations in the atmospheric boundary layer over Milan oasis are only caused by the oasis itself, and (b) free tropospheric NO_2 concentrations, which are usually due to large-scale tropospheric NO_2 advection, are negligible.

According to Koeppen classification (1931), Milan oasis owns a cold desert climate (BWk), which is dominated by long hot summers (30 years' mean: 29 °C) and cold

ACPD
14, 19357–19394, 2014

winters (30 years' mean: – 6 °C). Mean annual precipitation amounts 28.5 mm, mean annual evaporating capacity is 2920 mm, mean wind direction is NE to E, and mean wind speed 2.7 m s^{-1}.

2.2 In-situ measurements

A field campaign has been performed at Milan oasis, from 24 May to 26 June 2011. A total of 32 individual MAX-DOAS measurements (approx. 20 min) have been performed by two Mini-MAX-DOAS instruments (partially simultaneously) on 21 days during the 2011 campaign at the NE natural forest site (1), desert site (2), jujube site (3) and hotel station in Milan oasis center (4). Accompanying data of wind direction, wind speed, air temperature, barometric pressure, global and net radiation have been observed at sites (1)–(5) at 1.8 m above ground (at NW natural forest: 11 m; at hotel station: 23 m). Soil temperature (at 0.05 m depth), as well as rainfall (amount and intensity) were recorded at all sites in 2011.

2.2.1 Ground-based measurements of vertical column densities of NO_2

Multi-Axis-Differential Optical Absorption Spectroscopy (MAX-DOAS) observes scattered sun light under various (mostly slant) elevation angles. From combinations of the retrieved NO_2 slant column densities (SCDs) obtained at different elevation angles, information on the vertical NO_2 profile and/or on the corresponding vertical column density (VCD) can be obtained (Hönninger et al., 2002; Sinreich et al., 2005; Wittrock et al., 2004; Wagner et al., 2011). Spectral calibration of the MAX-DOAS instruments was performed by fitting a measured spectrum to a convoluted solar spectrum based on a high resolution solar spectrum (Kurucz et al., 1984). Several trace gas absorption cross sections of NO_2 at 294 K (Vandaele et al., 1996), H_2O at 290 K (Rothman et al., 2005), Glyoxal at 296 K (Volkamer et al., 2005), O_3 at 243 K (Bogumil et al., 2003) and O_4 at 286 K (Hermans et al., 1999) were convolved to match the resolution of the instrument and then used in the spectral analysis using a wavelength range of 420–450

ACPD
14, 19357–19394, 2014

(also a Ring spectrum was included in the fitting process). The output of the spectral analysis is the NO_2 SCD, which represents the NO_2 concentration integrated along the corresponding light paths through the atmosphere.

Since a spectrum measured in zenith direction (a so called Fraunhofer reference spectrum) is included in the fit process to remove the strong Fraunhofer lines, the retrieved NO_2 SCD actually represents the difference between the SCDs of the measurement and the Fraunhofer reference spectrum; it is usually referred to as differential SCD or $DSCD_{meas}$. The tropospheric DSCD for the elevation angle α can be derived from MAX-DOAS observation by subtracting the NO_2 DSCD for the closest zenith observation ($\alpha_0 = 90^\circ$):

$$DSCD_{trop}(\alpha) = DSCD_{meas}(\alpha) - DSCD_{meas}(\alpha_0) \quad (1)$$

DSCDs are converted into VCDs (the vertically integrated concentration) using so called air mass factors (AMF, Solomon et al., 1987), which is defined by:

$$AMF = SCD/VCD \quad (2)$$

In many cases AMF are determined from radiative transfer simulations (Solomon et al., 1987). However, if trace gas column densities are retrieved from MAX-DOAS observations at high elevation angles ($> 10^\circ$), the AMF can be determined by the so called geometric approximation (Hönninger et al., 2002; Brinksma et al., 2008; Wagner et al., 2010):

$$AMF_{trop} \approx \frac{1}{\sin(\alpha)} \quad (3)$$

In this study, the tropospheric vertical column density (VCD_{trop}) is obtained from $DSCD_{trop}(\alpha)$ as discussed by Wagner et al. (2010):

$$VCD_{trop} = \frac{DSCD_{trop}(\alpha)}{AMF_{trop}(\alpha - AMF_{trop}(\alpha_0))} \quad (4)$$

ACPD
14, 19357–19394, 2014

During the field experiments, the MAX-DOAS instruments have been mounted on solid tables (aluminium structure) at approx. 11 m a.gr. (NW natural forest, hotel station) and 3.5 m a.gr. (remainder of sites) with the telescope facing northwards. Observations were always made on elevation angles of 0°, 2°, 4°, 6°, 8°, 10°, 15°, 20°, 45° and 90°. VCD_{trop}s were determined from measurements at 15°. At such elevation angles, effects of scattering by air molecules and aerosols can be usually neglected. However, for comparison of the $DSCD_{trop}$ data obtained by MAX-DOAS with the simulated SCDs obtained from 3-D distributions of NO_2 concentration (calculated with LASAT on the basis of laboratory derived net potential NO_2 fluxes) the lower elevation angles (2°, 4°) for $DSCD_{trop}(\alpha)$ have been used, which have a much higher sensitivity to the observed NO_2.

For classifying all MAX-DOAS measurements whether they were made up-wind, down-wind, or in the center of Milan oasis, their observation position was related to the mean wind direction during each measurement period. Wind measurements were part of accompanying in situ measurements (see below).

2.2.2 Accompanying measurements

Wind direction, wind speed, air temperature, relative humidity, barometric pressure, and rainfall intensity have been measured by combined weather sensors (weather transmitter WXT510, Vaisala, Finland). All five weather sensors have been operated side-by-side for one week before they have been mounted at the individual measurement sites (1)–(5). Based on these results, all meteorological data, which have been measured between 3–24 July 2011 have been corrected using one of the sensors as reference. All combined weather sensors' data, as well as those of net radiation (4 component net radiation sensor, model NR01, Hukseflux, the Netherlands) and soil temperature (thermistor probe, model 109, Campbell Scientific, USA) have been recorded every minute. Ambient O_3 concentrations and NO_2 photolysis rates have also been measured in-situ; both quantities are necessary to calculate the $NO \rightarrow NO_2$ conversion factor (see Sect. 2.2.8). Ozone concentrations have been measured by UV-absorption

ACPD
14, 19357–19394, 2014

spectroscopy (model 49i, ThermoFisher Scientific, USA) and NO_2 photolysis rate by a filter radiometer (model 2-Pi-JNO_2, metcon, Germany) in 1 min intervals.

2.2.3 Soil samples

Microbial processes responsible for biogenic NO emission are confined to the uppermost soil layers (Galbally and Johansson, 1989; Rudolph et al., 1996; Rudolph and Conrad, 1996). Consequently, composite soil samples (1 kg of top soil, 0–5 cm depth) have been collected at the individual sites of Milan oasis (natural forest, cotton, jujube, cotton & jujube mixture, desert). All samples (air dried) were sent from Xinjiang to Germany by air cargo and stored refrigerated (+4 °C) until laboratory analysis of the net potential NO flux (see below). Sub-samples have been analyzed for dry bulk soil density (ISO 11272), pH (ISO 10390), electrical conductivity (salinity, ISO 11265), contents of nitrate and ammonium (ISO 14256), total carbon and total nitrogen (ISO 10649 and ISO 13878), texture (ISO 11277), as well of soil water potential (pF values 1.8, 2.5, 4.2, Hartge and Horn, 2009).

Electrical conductivity varied between 1.6 to 9.5 $dS\,m^{-1}$ within the managed soils, and was 59.8 and 3.0 $dS\,m^{-1}$ in the natural forest and desert soils, respectively. Commercially available soil moisture probes (e.g. TDR and FDR) show extreme interferences for soils of $> 2\,dS\,m^{-1}$ (cf. Kargas et al., 2013) and their calibration for such soils is extremely challenging, if possible at all. Indeed, FDR-signals monitored in Milan oasis' soils were extremely noisy and spurious. Nevertheless, up-scaling of the laboratory derived net potential NO fluxes needs data of the uppermost layer of each soil of Milan oasis land-types (see Sect. 2.2.6). For that, as most reasonable approximation, it was decided to use that individual (constant) gravimetric soil moisture content, which corresponds to the so-called "wilting point". The latter was determined by laboratory water tension measurements (pF 4.2) on undisturbed soil cores from each land-cover type. The wilting point is defined as that soil moisture in the root zone, which would cause irreversible wilting of plants. Wilting point conditions in the uppermost soil layers (2 cm) of soils in the Taklimakan Desert are easily reached, since evaporation there

ACPD
14, 19357–19394, 2014

is extremely high (evaporating capacity 2920 mm a^{-1}). Even after flooding irrigation of Milan oasis' crop fields, these conditions have repeatedly been observed within at least 3 days by visual inspections.

2.2.4 Laboratory determination of net potential NO_2 fluxes

The methodology for the laboratory measurement of the NO flux from soil has been developed at the end of the nineties (Yang and Meixner, 1997) and has been continuously used during the last two decades (Otter et al., 1999; Kirkman et al., 2001; van Dijk and Meixner, 2001; Feig et al., 2008a, b; Yu et al., 2008, 2010a, b; Ashuri, 2009; Feig, 2009; Gelfand et al., 2009; Bargsten et al., 2010). The methodology has been significantly improved in the frame of this study and is described in detail by Behrendt et al. (2014).

Generally, the release of gaseous NO from soil is the result of microbial NO production and simultaneous NO consumption. The latter is, as shown by Behrendt et al. (2014), particularly for arid and hyper-arid soils, negligible. Applying the laboratory dynamic chamber method, the release of NO is determined by incubating aliquots of the soil samples in a dynamic chamber system under varying, but prescribed conditions of soil moisture, soil temperature, and chamber's headspace NO concentrations. From the difference of measured NO concentrations at the outlets of each soil containing chamber and an empty reference chamber, actual net potential NO fluxes (in terms of mass of nitric oxide per area and time) is calculated as function of soil moisture and soil temperature. For that, a known mass (approx. 60 g dry weight) of sieved (2 mm) and wetted (to water holding capacity) soil is placed in one of six Plexiglas chambers (volume 9.7×10^{-4} m^3) in a thermo-controlled cabinet (0–40 °C). After passing through a purification system (PAG 003, Ecophysics, Switzerland), dry pressurized, zero (i.e., "NO free") air is supplied to each chamber, controlled by a mass flow controller (4.167×10^{-5} m^3 s^{-1}). The outlet of each chamber is connected via a switching valve system to the gas-phase chemiluminescence NO analyzer (model

ACPD
14, 19357–19394, 2014

42i-TL, Thermo Fisher Scientific Inc., USA) and to the non dispersive infrared analyzer CO_2/H_2O-analyzer (model LI-COR 840A, LI-COR Biosciences Inc., USA). During a period of 24–48 h, the soil samples are slowly drying out, hence providing the desired variation over the entire range of soil moisture (i.e. from water holding capacity to wilting point conditions and completely dry soil). During the drying out period, the temperature of thermo-controlled cabinet is repeatedly changed from 20 to 30 °C, hence providing the desired soil temperature variation. Occasionally, nitric oxide standard gas (200 ppm) is diluted into the air purification system via a mass flow controller; this allows the control of the chamber headspace NO concentration when determining NO consumption rate of the soil sample. The actual soil moisture content of each soil sample is determined by considering the H_2O mass balance of each chamber, where the temporal change of the chamber's headspace H_2O concentration is explicitly related to the evaporation rate of the soil sample. Tracking the chamber's headspace H_2O concentration throughout the drying-out period and relating it to the gravimetrically determined total soil mass at the start and end of the measurement period delivers the actual gravimetric soil moisture content of the soil sample (Behrendt et al., 2014).

As shown during the last two decades, the dependence of NO release from gravimetric soil moisture and soil temperature can be characterized by two explicit dimensionless functions, the so-called optimum soil moisture curve $g(\theta_g)$ and the exponential soil temperature curve $h(T_{soil})$

$$g(\theta_g) = \left(\frac{\theta_g}{\theta_{g,0}}\right)^a \exp\left[-a\left(\frac{\theta_g}{\theta_{g,0}} - 1\right)\right] \quad (5)$$

$$h(T_{soil}) = \exp\left[\frac{\ln Q_{10,NO}}{10}\left(T_{soil} - T_{soil,0}\right)\right] \quad (6)$$

where θ_g is the dimensionless gravimetric soil moisture content, $\theta_{g,0}$ the so-called optimum gravimetric soil moisture content (i.e., where the maximum NO release has been observed), a is the soil moisture curve's shape factor (solely derived from NO release

ACPD
14, 19357–19394, 2014

and gravimetric soil moisture data which have been observed during the drying-out measurements, see Behrendt et al., 2014), T_{soil} is the soil temperature (in °C), $T_{soil,0}$ is the reference temperature (here: 20 °C), and $Q_{10,NO}$ is the (logarithmic) slope of $h(T_{soil})$, defined by

$$Q_{10,NO} = \frac{\ln F_{NO}\left(\theta_{g,0}, T_{soil,1}\right) - \ln F_{NO}\left(\theta_{g,0}, T_{soil,0}\right)}{T_{soil,1} - T_{soil,0}} \quad (7)$$

where $T_{soil,1}$ is a soil temperature which is 10 K different from $T_{soil,0}$ (here: 30 °C). The actual NO fluxes F_{NO} (ng m^{-2} s^{-1}; in terms of mass of nitric oxide) are defined by

$$F_{NO}\left(\theta_{g,0}, T_{soil,0}\right) = \frac{Q}{A_{soil}}\left[m_{NO,cham}\left(\theta_{g,0}, T_{soil,0}\right) - m_{NO,ref}\right] f_{C,NO} \quad (8)$$

$$F_{NO}\left(\theta_{g,0}, T_{soil,1}\right) = \frac{Q}{A_{soil}}\left[m_{NO,cham}\left(\theta_{g,0}, T_{soil,1}\right) - m_{NO,ref}\right] f_{C,NO} \quad (9)$$

where Q is the purging rate of the dynamic chambers (m^3 s^{-1}), A_{soil} is the cross-section of the dynamic chamber (m^2), and $m_{NO,cham}$ and $m_{NO,ref}$ are the NO mixing ratios (ppb) observed under conditions ($\theta_{g,0}$,$T_{soil,0}$) and ($\theta_{g,0}$,$T_{soil,1}$) at the outlets of each soil chamber and the reference chamber, respectively. The conversion of NO mixing ratios to corresponding NO concentrations (ng m^{-3}, in terms of mass of nitric oxide) is considered by $f_{C,NO}$ (= 572.5 ng m^{-3} ppb^{-1} under STP conditions). Finally, the net potential NO flux, $F_{NO}(\theta_g, T_{soil})$ is given by

$$F_{NO}\left(\theta_g, T_{soil}\right) = F_{NO}\left(\theta_{g,0}, T_{soil,0}\right) g\left(\theta_g\right) h\left(T_{soil}\right) \quad (10)$$

This net potential NO flux is specific for each soil sample, hence for sites (1), (2), (4), and (5) of Milan oasis; the actual NO flux of the sites is calculated applying corresponding field data of gravimetric soil moisture and soil temperature. This procedure has been successfully applied for a variety of terrestrial ecosystems (e.g., Otter et al., 1999; van

ACPD
14, 19357–19394, 2014

Dijk et al., 2002; Ganzeveld et al., 2008). For soils of the Zimbabwean Kalahari (Ludwig et al., 2001; Meixner and Yang, 2006), for a German grassland soil (Mayer et al., 2011), but also for Brazilian rainforest soils (van Dijk et al., 2002), soil biogenic NO fluxes derived from the described laboratory incubation method have been successfully verified by field measurements using both, field dynamic chamber and micrometeorological (aerodynamic gradient) techniques.

2.2.5 Classification and actual distribution of Milan fields

Image classification is likely to assemble groups of identical pixels found in remotely sensed data into classes that match the informational categories of user interest by comparing pixels to one another and to those of known identity. For the purposes of our study, land-cover classification was carried out based on two Quickbird images (0.6 m ground resolution, DigitalGlobe, http://www.digitalglobe.com) acquired on 9 April and 31 August 2007 respectively, with the aid of a recent ETM+ Landsat image (141/033, http://earthexplorer.usgs.gov/) acquired on 25 April 2011 (15 and 30 m spatial resolution). A major advantage of using Quickbird images of high spatial resolution images is that such data greatly reduce the mixed-pixel problem (a "mixed pixel" consists of several land-cover classes) and provide a greater potential to extract much more detailed information on land-cover structures (e.g. field borders, buildings, roads) than medium or coarse spatial resolution data using whether on screen digitizing or image classification.

However, we take the advantage of resolution merge processing to increase the spatial resolution of the Landsat image from 30 to 15 m for the bands 1–5 and 7 for better land-cover mapping and for updating the land-cover map from 2007 to 2011. Then, we defined different areas of interests (AOIs) to represent the major land-covers with the aid of in-situ GPS data collection (45 points). Next, we increased number of AOIs based on image spectral analysis method. After that supervised classification was performed using the maximum likelihood parametric rule and probabilities. This classifier uses the training data by means of estimating means and variances of the classes,

ACPD
14, 19357–19394, 2014

which are used to estimate Bayesian probability and also consider the variability of brightness values in each class. For that, it is the most powerful classification methods when accurate training data is provided and one of the most widely used algorithms (Perumal and Bhaskaran, 2010). As a result, five major ecosystems were determined: cotton, jujube, cotton/jujube mixture fields, desert, and plant cover). The cotton and the jujube fields are the most dominant types. Finally, the classified land-cover image was converted into vector format using polygon vector data type to be implemented in LASAT analysis as sources of NO flux and for the purpose of estimating NO concentrations. The map includes 2500 polygons of different sizes as sub-units of Milan major land-cover.

2.2.6 Two dimensional distribution of soil NO emissions of Milan oasis

The soil NO emission sources of Milan oasis were defined by individual source units, which have been identified as those sub-units (polygons) of the land-cover vector map consisting of natural forest or desert, or covered by cotton, jujube, cotton/jujube mixture. Two identifiers have been attributed to each source unit, (a) a metric coordinate whose numerical format refers to the corner of the corresponding polygon, and (b) a unique ID number followed by a description of its land cover type. The soil NO source strength (i.e., actual NO flux, see Sect. 2.2.4) of each source unit has been calculated from the corresponding net potential NO flux, the land-cover type specific gravimetric soil moisture content ("wilting point"), and the actual soil temperature, which has been in situ measured for each of the land-cover types of Milan oasis (see Sect. 2.2.2). Those polygons which are not matching the mentioned land-cover types and other tiny polygons generated by digital image processing techniques were dismissed to avoid intricate geometric errors affecting NO emission data. In other words, these "other classes" were dissolved before performing LASAT analysis to avoid extreme values.

ACPD
14, 19357–19394, 2014

2.2.7 Three dimensional distribution of NO concentrations by Lagrangian dispersion modelling (LASAT)

Having the actual NO source units of the Milan oasis available, the 3-D distribution of NO concentrations in the atmospheric boundary layer (0–1500 m a.gr.) over Milan oasis have been calculated by the state-of-art Lagrangian dispersion model LASAT (German VDI Guidelines VDI3945, part 3; cf. Janicke Consulting, 2011). For that, pre-processing of meteorological parameters (i.e. 3-D wind distribution, based on meteorological in situ measurements, see Sect. 2.2.2) and calculation of dispersion parameters (σ_y, σ_z) have to be performed. Unfortunately, it was difficult to obtain fine resolution using LASAT individually. Therefore, LASAT model was integrated with Geographic Information System (ArcGIS) by using an advanced module namely LASarc (IVU Umwelt GmbH, 2012). LASarc allowed us to calculate NO concentrations using relatively fine resolution of 30 m × 30 m and taking the advantages of using integrated map colour scheme in ArcGIS. This module has been used to realize Milan oasis' complex NO source configuration and to setup calculations of LASAT.

The model was designed to calculate NO-concentrations at 16 different vertical layers (0–3, 3–5, 5–10, 10–20, 20–30, 30–50, 50–70, 70–100, 100–150, 150–200, 200–300, 300–400, 400–500, 500–700, 700–1000, and 1000–1500 m a.gr.). The horizontal resolution is 30 m, in x-direction (W–E) as well in y-direction (S–N), which results in 656 (x) and 381 (y) grids for the Milan oasis domain. LASAT's meteorological input data contain a variety of parameters, namely start and end time (T_1, T_2), wind speed (U_a) and wind direction (R_a) at anemometer height (H_a), average surface roughness (Z_0), and atmospheric stability (in terms stability classes). These parameters have been provided in a time-dependent tabular form, up-dated every 30 min (except Z_0). Average (30 min) wind speed and wind direction data have been calculated from in situ measurements (1 min resolution, see Sect. 2.2.2).

ACPD
14, 19357–19394, 2014

LASAT's pre-processing module determines the vertical profile of wind speed according to the well-known logarithmic relation,

$$U(z) = \frac{u_*}{k} \ln\left(\frac{z}{Z_0}\right) \tag{11}$$

where $U(z)$ is the horizontal wind speed ($\mathrm{m\,s^{-1}}$) at height z (m), u_* is the friction velocity ($\mathrm{m\,s^{-1}}$), k is the dimensionless von Karman constant (= 0.4, Simiu and Scanlan, 1996), and Z_0 is the surface roughness length (m). LASAT's pre-processing module accepts only one individual value for Z_0; nevertheless, the required mean value has been calculated from all Z_0's of Milan oasis domain, which have been assigned to each of the sub-units (polygons) of the vector land-cover map (see Sect. 2.2.5). For individual Z_0's, we calculated land-cover specific NDVI data (normalized differential vegetation index) from Landsat ETM+ image (141/033)

$$\mathrm{NDVI} = \frac{r_{\mathrm{NIR}} - r_{\mathrm{RED}}}{r_{\mathrm{NIR}} + r_{\mathrm{RED}}} \tag{12}$$

where NIR is the reflectance in the near-infrared bandwidth (0.77–0.90 µm) and RED is the reflectance in the red bandwidth (0.63–0.69 µm). In Landsat ETM+ images, these correspond to bands 4 and 3, respectively. Finally, r_{NIR} and r_{RED} are the corresponding ratios of reflected and incident energy as a function of wavelength (see Chander and Markham, 2003). Then, surface roughness grid data was estimated as:

$$Z_0(x,y) = \exp\left(a_{xy}\,\mathrm{NDVI}(x,y) + b_{xy}\right) \tag{13}$$

where a_{xy} and b_{xy} are constants, which are, according to Morse et al. (2000), derived from NDVI(x, y) and GPS(x, y) data for known sample pixels representing the earlier classified land-cover types, namely natural forest, desert, cotton, jujube, and cotton/jujube mixture. Corresponding land-cover type Z_0's are 0.45, 0.01, 0.18, 0.26, and 0.22 m, respectively; the required average value over the entire LASAT model domain results in $Z_0 = 0.22 \pm 0.158$ m.

ACPD
14, 19357–19394, 2014

Besides mechanical turbulence (Z_0), atmospheric stability affects most the dispersion of trace substances. For Milan oasis' atmospheric boundary layer, atmospheric stability has been calculated according to the "solar radiation/delta T (SRDT)" method in 30 min intervals. This method (cf. Turner, 1994) is widely accepted because of its simplicity and its representativeness for atmospheric stability over open country and rural areas, like the Milan oasis domain. Daytime stability classes are calculated from in situ measurements of solar radiation and horizontal wind speed (see Sect. 2.2.2).

Finally, 30 min means of all parameters and input variables of LASAT have been calculated. Using these, about 4×10^6 gridded data points of 3-D NO concentration have been calculated for each time period considered in Sect. 3.2.

2.2.8 Simulation of SCD_{NO_2} and VCD_{NO_2} by spatial integration of LASAT results

There is only one tool to provide a robust relationship between biogenic soil NO emissions on one hand and MAX-DOAS observed SCDs and VCDs on the other hand: the exact simulation of the MAX-DOAS measurement through spatial integration of three dimensional NO concentrations calculated by LASAT (followed by NO→NO_2 conversion). At a given location of the MAX-DOAS measurement, integration must be performed from the height where the MAX-DOAS instrument has been set-up ($h_{MAXDOAS}$) to the end of the atmospheric boundary layer (h_{ABL} = 1500 m a.gr.) along two virtual light paths, (a) the vertical up path (VCD), and (b) the slant path (SCD) according to the selected elevation angle of each MAX-DOAS measurement.

Calculation of simulated VCD's for NO ($VCD_{NO,sim}$) at the location of a MAX-DOAS instrument is achieved as follows: (a) determination of the NO mass density (ng m^{-2}) of the vertical column between $h_{MAXDOAS}$ and h_{ABL}; this is obtained by adding NO concentrations (ng m^{-3} in terms of mass of nitric oxide) of all LASAT cells in vertical direction over that 30 m × 30 m grid, which contains the location of the MAX-DOAS instrument, multiplied by the height difference $\Delta h = h_{ABL} - h_{MAXDOAS}$ (in m), (b) multiplying that NO mass density by the ratio of Avogadro's number (6.02217×10^{26} molecules $kmol^{-1}$) and

ACPD
14, 19357–19394, 2014

the molecular weight of NO (30.0061×10^{12} ng kmol^{-1}) delivers the desired value of $VCD_{NO,sim}$ in units of molecules m^{-2} ($\times 10^{-4}$: molecules cm^{-2}) at the location of the MAX-DOAS instrument. Calculation of simulated SCD's for NO ($SCD_{NO,sim}$) requires the determination of the 3-D light path through the trace gas layered. Positioning of MAX-DOAS's telescope was always to the north, the selected MAX-DOAS elevation angle α and h_{ABl} deliver the length of the slant light path ($= h_{ABL}/\sin\alpha$). The desired $SCD_{NO,sim}$ (in molecules m^{-2}) results from the NO mass density of the slant column multiplied by the length of the slant light path, where the NO mass density is equivalent to the sum of all NO concentrations of those LASAT cells which are intersected by the slant light path from the position of the MAX-DOAS instrument to h_{ABL}.

For conversion of $VCD_{NO,sim}$ to $VCD_{NO_2,sim}$ and $SCD_{NO,sim}$ to $SCD_{NO_2,sim}$ it is assumed, that the photostationary state (PSS) of the triad NO, NO_2, and O_3 is established in Milan oasis' atmospheric boundary layer. According to Leighton (1961) this chemical equilibrium state is due to fast photochemical reactions, namely $NO + O_3 \rightarrow NO_2 + O_2$ and $NO_2 + h\upsilon \rightarrow NO + O$, from which the so-called photostationary state NO_2 concentration ($NO_{2,PSS}$) can be derived as

$$[NO_{2,PSS}] = \frac{[O_3][NO]k_1}{j(NO_2)} \tag{14}$$

where $[O_3]$ is the ozone number density (molecules cm^{-3}; calculated from in situ measured O_3 concentrations, see Sect. 2.2.2), [NO] is the NO number density, k_1 is the reaction coefficient of the $NO + O_3 \rightarrow NO_2 + O_2$ reaction (cm^3 molecules^{-1} s^{-1}; Atkinson et al., 2004), and $j(NO_2)$ is the in situ measured NO_2 photolysis rate (in s^{-1}; see Sect. 2.2.2). Finally, $VCD_{NO_2,sim}$ and $SCD_{NO_2,sim}$ are calculated from $VCD_{NO,sim}$ and $SCD_{NO,sim}$ by

$$VCD_{NO_2,sim} = CF_0 \times VCD_{NO,sim} \text{ and } SCD_{NO_2,sim} = CF_0 \times SCD_{NO,sim} \tag{15}$$

where the $NO \rightarrow NO_2$ conversion factor is defined by $CF_0 = [O_3]k_1/j(NO_2)$.

ACPD
14, 19357–19394, 2014

3 Results and Discussion

3.1 Land-cover type specific net potential NO fluxes

Net potential NO fluxes (as functions of soil temperature and moisture) have been determined by incubation of samples which have been taken from the top-soil of Milan oasis' major land-cover types, i.e. natural forest, desert, cotton, jujube, and cotton/jujube mixture (see Sect. 2.2.4). Figure 2 shows the laboratory derived net potential net NO flux, F_{NO} from soils of the most contrasting land-cover types of Milan oasis (irrigated and fertilized fields of cotton, jujube, cotton/jujube mixture, and desert).

Net potential NO fluxes of the natural forest land-cover type are not shown, because laboratory incubation measurements have shown that there is no significant NO release from these soils, most likely due to its high electrical conductivity (salt content). Optimum gravimetric soil water contents (i.e., where the maximum of F_{NO} is observed) for desert, managed cotton, and managed jujube soils have one in common, very low values of $\theta_{g,\,opt}$ (0.009–0.017) for soil temperatures of 50 °C. During the vegetation period (April–September), soil temperatures of > 40 °C are easily reached for the soils of Milan oasis, particularly for the desert soils. While the nature of all Milan oasis' soils is arid/hyper-arid, maximum net potential NO fluxes are 7600, 63, 270, and 98 ng m^{-2} s^{-1} (in terms of mass of nitric oxide) for cotton, jujube, jujube/cotton mixture, and desert soils, respectively.

3.2 Land-cover types of Milan oasis and actual NO fluxes

As mentioned in Sect. 2.2.5, land-cover classification and actual distribution of Milan oasis' fields have been identified from satellite images (Quickbird, Landsat ETM+). The 2011 distribution of fields and the corresponding land-cover is shown in Fig. 3.

The dominant crop was cotton, representing 18 % (64 km^2) of the total field area of Milan oasis (jujube 7 %, 28 km^2), cotton/jujube mixture 0.89 % (3 km^2), natural forest 18 % (64 km^2), residential area 1.62 % (5.5 km^2) and desert 52 % (174 km^2).

ACPD
14, 19357–19394, 2014

Land-cover specific, actual NO fluxes (30 min means) from cotton, jujube, cotton/jujube, and desert soils were calculated from corresponding laboratory derived net potential NO fluxes, land-type specific soil moisture and soil temperature data (see Sect. 2.2.6). These NO fluxes (ng m^{-2} s^{-1}, in terms of mass of nitric oxide) were then assigned to each individual source unit (i.e. to each of the 2500 polygons of Milan oasis' domain). For the period 08:30–14:30 on 9 June 2011, for example, the "land-cover cotton" NO flux ranged from 21–64 ng m^{-2} s^{-1} (in terms of NO). The soil biogenic NO emission from all cotton fields between 08:30 and 14:30 was estimated to 28.7 kg (in terms of NO), equivalent to 76 % of the total soil biogenic NO emission of the entire Milan oasis.

3.3 Vertical NO_2 column densities by MAX-DOAS

We performed 32 individual MAX-DOAS measurements within 21 days of the 2011 field campaign to examine the spatial variation between the observed sites. In Fig. 4, all observed vertical NO_2 column densities (in molecules cm^{-2}) observed at sites (1)–(4) of Milan oasis are shown in polar coordinates with reference to corresponding wind directions measured in situ at the individual sites.

Wind speeds (30 min means) ranged between 1.5 and 5.7 m s^{-1} and wind direction was mostly (78 %) from the northern quadrants (59 %, 9 %, 13 %, and 19 % from NE, SE, SW, and NE quadrants, respectively). As expected, highest VCDs (10^{15}–10^{16} molecules cm^{-2}) were observed at site (4) (Milan oasis center), regardless of wind direction. When the wind direction is from the NE quadrant, site (3) (jujube fields) is down-wind of Milan oasis (see Fig. 1); then its VCDs are as high as those obtained in the oasis' center ($5–7 \times 10^{15}$ molecules cm^{-2}). The few VCD data points of 1×10^{15} molecules cm^{-2} at the jujube site, attributed to winds from SE and SW quadrants, are mainly due to NO emissions from traffic on the National Road 315 which passes the southern margins of Milan oasis. Lowest VCDs (3×10^{13}–3×10^{14} molecules cm^{-2}) have been observed at site (1) (natural forest) and site (2) (desert). Alone from these spatially resolved VCD observations in the Milan oasis'

ACPD
14, 19357–19394, 2014

domain, the increase of VCD due to the oasis itself can be estimated in the order of at least one order of magnitude.

Fortunately, we have been able to perform simultaneous measurements with two MAX-DOAS instruments at sites (1) and (3) on 9 and 13 June 2011. Since winds (approx. 3 m s^{-1}) were from the NE quadrant during these two days, site (1) has been up-wind, and site (3) downwind of Milan oasis. Corresponding VCD results are shown in Fig. 5. NO_2 VCDs at the downwind site exceeded those at the upwind site by factors 5–9. This difference between downwind and upwind MAXDOAS signals is considered to be a direct measure for the areal increase of ambient NO_2 concentration. In the absence of anthropogenic NO_x sources (see Sect. 2.1), this provides first evidence for the considerable impact of the biogenic NO emissions from the fields of Milan oasis.

3.4 3-D distribution of ambient NO-concentration

The LASAT model has to be used to calculate the dispersion of soil emitted NO into the atmospheric boundary layer over Milan oasis. An example for the resulting distribution of NO the concentration in the first four vertical layers of LASAT (0–3, 3–5, 5–10, and 10–20 m) is shown in Fig. 6 (9 June 2011; 11:30–13:00 local time). The shown results are the mean of three LASAT model runs, since a new LASAT calculation of 3-D distribution of NO concentration is started for every set of meteorological parameters which are provided every 30 min from means of the in situ measured meteorological quantities (see Sect. 2.2.2). During 11:30–13:00, mean wind direction was 15°, 38°, and 50°, wind speed was rather constant (2.60–2.67 m s^{-1}), and atmospheric stability class has been generally neutral (3.2).

By comparing the NO ambient concentrations, particularly in the first vertical LASAT layer (0–3 m) of oasis area with the surrounding desert, it becomes obvious that the great differences of ambient NO concentrations mirror the corresponding differences of actual soil NO fluxes from each source-unit; within this layer calculated mean NO concentrations are 13, 12, 10, and 1 ng m^{-3} (in terms of mass of nitric oxide; or 10.6, 9.8, 8.2, and 0.8 ppb) for the oasis centre, jujube fields, cotton/jujube mixture, and

ACPD
14, 19357–19394, 2014

desert, respectively. The value at the oasis center exceeds those over desert by more than an order of magnitude, similar as the corresponding VCD values (see above). As expected under the prevailing conditions of well developed atmospheric turbulence, NO concentrations rapidly decreases with height (see panels "0–3 m", "3–5 m", "5–10 m" in Fig. 6), and with prevailing northerly winds, the NO concentration center shifting southwards with increasing altitude.

3.5 Simulated SCDs and VCDs vs. SCDs and VCDs by MAX-DOAS

For those periods where simultaneous "upwind" and "downwind" MAX-DOAS measurements have been performed (9 and 13 June 2011), corresponding SCD_{sim} and VCD_{sim} have been simulated by suitable vertical integration (see Sect. 2.2.8) of LASAT-calculated 3-D NO concentrations, followed by NO → NO_2 conversion (based on photostationary state assumption of Milan oasis' atmospheric boundary layer). Since SCD_{sim} and VCD_{sim} represent only that part of true SCDs and VCDs of NO_2, which are due to the contribution of the oasis' soil NO emissions, SCD_{sim} and VCD_{sim} are compared to the difference of those SCDs and VCDs which have been simultaneously measured by two MAX-DOAS instruments at corresponding "downwind" and "upwind" sites (see Fig. 7). For elevation angles of 2° and 4°, SCD_{sim} and $\Delta SCD = SCD_{down} - SCD_{up}$ are shown in Fig. 7a. In Fig. 7b, VCD_{sim} and $\Delta VCD = VCD_{down} - VCD_{up}$ are shown for 15° elevation. There is remarkable good agreement between measured and simulated data. Since soil NO emission data used in the LASAT dispersion model were calculated from land-cover type specific potential net NO fluxes, which in turn were derived from laboratory incubation experiments on corresponding soil samples, the results in Fig. 7 are also considered as an excellent quality assurance of the chosen up-scaling of laboratory results to the oasis scale.

ACPD
14, 19357–19394, 2014

4 Conclusion

This study has been focused on the following activities: (1) representative soil sampling from the uppermost soil layer (< 0.05 m) of all land-cover type units (natural forest, cotton fields, jujube fields, cotton/jujube mixture, desert) of Milan oasis (Xinjiang, NW China), (2) laboratory incubation experiments (dynamic chamber system) to characterize the biogenic NO emission from these soil samples in form of net potential NO fluxes as function of soil moisture and soil temperature, (3) determination of the actual size, areal distribution, and land-cover type of Milan oasis' field units from satellite remote sensing information, (4) field measurements of slant (SCD) and vertical (VCD) NO_2 column densities (by MAX-DOAS) and additional quantities (soil moisture, soil temperature, ozone concentration, NO_2 photolysis rate, meteorological parameters) during an extended field campaign of 4 weeks at Milan oasis, (5) using data from (2), (3) and (4): calculation of Milan oasis' 2-D distribution of actual, land-cover specific NO fluxes, (6) calculation of 3-D NO concentrations in Milan oasis' atmospheric boundary layer originating from the dispersion of biogenic NO soil emissions determined by (5) with help of the Lagrangian dispersion model LASAT, (7) simulation of SCDs and VCDs by suitable vertical integration of calculated 3-D NO concentrations followed by suitable $NO \rightarrow NO_2$ conversion factors derived from in situ measurements, (8) comparison of measured and simulated SCDs and VCDs.

Results of the laboratory derived NO fluxes have shown that the extensively managed (fertilized and efficiently irrigated) cotton fields of Milan oasis release large amounts of soil biogenic NO; NO fluxes range between 10–30 $ng\,m^{-2}\,s^{-1}$ (in terms of mass of N), that is approx. 5–10 times more than from a typical central European wheat field).

Applying two MAX-DOAS instruments, simultaneous measurements have been performed at upwind and downwind sites of Milan oasis. Downwind site VCDs exceeded those from the upwind site by factors 5–9. Differences of VCD and SSC ("downwind" minus "upwind") are a direct measure for the areal increase of ambient NO_2

ACPD
14, 19357–19394, 2014

concentration caused by the oasis itself. The measured differences of VCDs and SCDs were compared with the simulated VCDs and SCDs and excellent agreement was found.

This agreement is considered as the first successful attempt to prove the validity of the chosen approach to up-scale laboratory derived biogenic NO fluxes to ecosystem level field conditions, i.e. from the spatial scale of a soil sample (cm^2) to field size (ha), and from field size (ha) to the size of an entire (agro-) ecosystem (km^2). Furthermore, in the absence of anthropogenic NO sources of Milan oasis (hydropower energy, battery powered trikes), it is obvious, that the areal increase of ambient NO_2 concentration in the atmospheric boundary layer of the isolated (in terms of NO_2 advection) Milan oasis is entirely due to biogenic NO emission from the arid/hyper-arid soils of the oasis itself. Extensive agricultural management of Milan oasis' crop fields (fertilization (350–600 kg N ha^{-1} a^{-1}) and effective irrigation of cotton and jujube fields) obviously provides considerable contribution of biogenic NO_x ($NO+NO_2$) from arid/hyper-arid soils of the Taklimakan desert to the local tropospheric NO_x budget.

About 80 % of the Chinese cotton production originates from the 3000 km long belt of oases surrounding Taklimakan Desert (1.65×10^6 km^2) in Xinjiang (NW-China); cotton cultivated land area in Xinjiang occupies the first place of entire China. Since 1955; Xinjiang's output of cotton increased 294 times (Lei et al., 2005). Fast economic growth in the region (+11 % GDP a^{-1}), inevitably accompanied by large anthropogenic NO_x emissions (traffic, energy production), may be countervailed or even exceeded by the "hotspot" character of Xinjiang's oases, namely by soil biogenic NO emissions from agriculturally dominated oases. Most likely, they will contribute most to the regional tropospheric NO_x budget. This is all the more likely, given the continued intensification of oasis agriculture around the Taklimakan desert which will be accompanied by corresponding land use change (desert → dryland farming with irrigation) in the coming decades.

Acknowledgements. This work was funded through the German Research Foundation (DFG) project "DEQNO – Desert Encroachment in Central Asia – Quantification of soil biogenic

ACPD
14, 19357–19394, 2014

Nitric Oxide" (DFG-MA 4798/1-1), the Max Planck Society (MPG), and the Max Planck Graduate Centre with Johannes Gutenberg-University Mainz (MPGC). The authors like to thank Guozheng Song, Günter Schebeske, Achim Zipka, Yanhong Li, Fanxia Wang, Aixia Yang, Sijun Luo, and Zhilin Zhu for their field assistance and their substantial support before, during, and after the DEQNO 2011 campaign. We also thank Reza Shaiganfar and Steffen Beirle for their supports during the pre-preparation of MAX-DOAS instrument.

The service charges for this open access publication have been covered by the Max Planck Society.

References

Ashuri, F. A.: Der Austausch von Stickstoffmonoxid zwischen Boden und Atmosphäre unter besonderer Berücksichtigung des Bodenwassergehaltes, Einfluss kulturlandschaftlicher Verhältnisse auf den Umsatz eines Spurengases. Ph.D. thesis, Johannes Gutenberg University Mainz, Mainz, Germany, 1–169, 2009.

Atkinson, R., Baulch, D. L., Cox, R. A., Crowley, J. N., Hampson, R. F., Hynes, R. G., Jenkin, M. E., Rossi, M. J., and Troe, J.: Evaluated kinetic and photochemical data for atmospheric chemistry: Volume I – gas phase reactions of O_x, HO_x, NO_x and SO_x species, Atmos. Chem. Phys., 4, 1461–1738, doi:10.5194/acp-4-1461-2004, 2004.

Bargsten, A., Falge, E., Pritsch, K., Huwe, B., and Meixner, F. X.: Laboratory measurements of nitric oxide release from forest soil with a thick organic layer under different understory types, Biogeosciences, 7, 1425–1441, doi:10.5194/bg-7-1425-2010, 2010.

Behrendt, T., Veres, P. R., Ashuri, F., Song, G., Flanz, M., Mamtimin, B., Bruse, M., Williams, J., and Meixner, F. X.: Characterisation of NO production and consumption: new insights by an improved laboratory dynamic chamber technique, Biogeosciences Discuss., 11, 1187–1275, doi:10.5194/bgd-11-1187-2014, 2014.

Beirle, S., Platt, U., Wenig, M., and Wagner, T.: Highly resolved global distribution of tropospheric NO_2 using GOME narrow swath mode data, Atmos. Chem. Phys., 4, 1913–1924, doi:10.5194/acp-4-1913-2004, 2004.

Bogumil, K., Orphal, J., Homann, T., Voigt, S., Spietz, P., Fleischmann, O. C., Vogel, A., Hartmann, A., Kromminga, H., Bovensmann, H., Frerick, J., and Burrows, J. P.: Measurements

ACPD
14, 19357–19394, 2014

of molecular absorption spectra with the SCIAMACHY pre-flight model: instrument characterization and reference data for atmospheric remote-sensing in the 230–2380 nm region, J. Photoch. Photobio. A, 157, 167–184, 2003.

Brinksma, E. J., Pinardi, G., Volten, H., Braak, R., Richter, A., Schoenhardt, A., Van Roozendael, M., Fayt, C., Hermans, C., Dirksen, R. J., Vlemmix, T., Berkhout, A. J. C., Swart, D. P. J., Oetjen, H., Wittrock, F., Wagner, T., Ibrahim, O. W., Leeuw, G. de., Moerman, M., Curier, R. L., Celarier, E. A., Cede, A., Knap, W. H., Veefkind, J. P., Eskes, H. J., Allaart, M., Rothe, R., Piters, A. J. M., and Levelt, P. F.: The 2005 and 2006 DANDELIONS NO_2 and aerosol intercomparison campaigns, J. Geophys. Res., 113, 1–18, 2008.

Chameides, W. L., Fehsenfeld, F., Rodgers, M. O., Cardelino, C., Martinez, J., Parrish, D., Lonneman, W., Lawson, D. R., Rasmussen, R. A., Zimmerman, P., Greenberg, J., Middleton, P., and Wang, T.: Ozone precursor relationships in the ambient atmosphere, J. Geophys. Res., 92, 6037–6055, 1992.

Chander, G. and Markham, B.: Revised Landsat-5 TM radiometric calibration procedures and postcalibration dynamic ranges, IEEE T. Geosci. Remote, 41, 2674–2677, 2003.

Conrad, R.: Soil Microorganisms as controllers of atmospheric trace gases (H_2, CO, CH_4, COS, N_2O and NO), Microbiol. Rev., 60, 609–640, 1996.

Crutzen, P. J.: Role of the tropics in atmospheric chemistry, in: The Geophysiology of Amazonia, edited by: Dickinson, R. E., John Wiley & Sons, New York, 107–132, 1987.

Davidson, E. A. and Kingerlee, W.: A global inventory of nitric oxide emissions from soils, Nutr. Cycl. Agroecosys., 48, 37–50, 1997.

Denman, K. L., Brasseur, G. P., Chidthaisong, A., Ciais, P., Cox, P. M., Dickinson, R. E., Hauglustaine, D., Heinze, C., Holland, E. A., Jacob, D. J., Lohmann, U., Ramachandran, S., Da Silva Dias, P. L., Wofsy, S. C., and Zhang, X.: Couplings between changes in the climate system and biogeochemistry, in Climate Change 2007: The physical science basis. Contribution of working group 1 to the fourth assessment report of the Intergovernmental Panel on Climate Change, edited by: Solomon, S., Qin, D., Manning, M., Chen, Z., Marquis, M., Averyt, K. B., Tignor, M., Miller, H. L., Cambridge University Press, Cambridge, 499-588, 2007.

Feig, G. T.: Soil Biogenic Emissions of Nitric Oxide from Arid and Semi-Arid Ecosystems, Ph.D. thesis, Johannes Gutenberg University Mainz, Mainz, Germany, 1–222, 2009.

ACPD
14, 19357–19394, 2014

Feig, G. T., Mamtimin, B., and Meixner, F. X.: Soil biogenic emissions of nitric oxide from a semi-arid savanna in South Africa, Biogeosciences, 5, 1723–1738, doi:10.5194/bg-5-1723-2008, 2008a.
Feig, G. T., Mamtimin, B., and Meixner, F. X.: Use of laboratory and remote sensing techniques to estimate vegetation patch scale emissions of nitric oxide from an arid Kalahari savanna, Biogeosciences Discuss., 5, 4621–4680, doi:10.5194/bgd-5-4621-2008, 2008b.
Galbally, I. E. and Johansson, C.: A model relating laboratory measurements of rates of nitric oxide production and field measurements of nitric oxide emissions from soils, J. Geophys. Res., 94, 6473–6480, 1989.
Ganzeveld, L., Eerdekens, G., Feig, G., Fischer, H., Harder, H., Königstedt, R., Kubistin, D., Martinez, M., Meixner, F. X., Scheeren, H. A., Sinha, V., Taraborrelli, D., Williams, J., Vilà-Guerau de Arellano, J., and Lelieveld, J.: Surface and boundary layer exchanges of volatile organic compounds, nitrogen oxides and ozone during the GABRIEL campaign, Atmos. Chem. Phys., 8, 6223–6243, doi:10.5194/acp-8-6223-2008, 2008.
Gelfand, I., Feig, G., Meixner, F. X., and Yakir, D.: Afforestation of semi-arid shrubland reduces biogenic NO emission from soil, Soil Biol. Biochem., 41, 1561–1570, 2009.
Harrison, P. and Pearce, F.: Deserts and Drylands, AAAS Atlas of Population and Environment, University of California Press, Berkeley, USA, 131–134, 2000.
Hartge, H. and Horn, R.: Die physikalische Untersuchung von Böden: Praxis Messmethoden Auswertung, Schweizerbartsche Verlagsbuchhandlung, Stuttgart, Germany, 1–178, 2009.
Hermans, C., Vandeale, A. C., Carleer, M., Fally, S., Colin, R., Jenouvrier, A., Coquart, B., and Merienne, M. F.: Absorption Cross-Sections of Atmospheric Constituents, NO_2, O_2, and H_2O, Environ. Sci. Pollut. Res., 6, 151–158, 1999.
Hönninger, G. and Platt, U.: The Role of BrO and its Vertical Distribution during Surface Ozone Depletion at Alert, Atmos. Environ., 36, 2481–2489, 2002.
Hönninger, G., von Friedeburg, C., and Platt, U.: Multi axis differential optical absorption spectroscopy (MAX-DOAS), Atmos. Chem. Phys., 4, 231–254, doi:10.5194/acp-4-231-2004, 2004.
IVU Umwelt GmbH: LASarc – GIS integration of LASAT, Environmental Planning and Information Systems, Freiburg, Germany, 2012.
Janicke Consulting: Dispersion model LASAT, Version 3.2, Reference Book, Janicke Consulting, Überlingen, Germany, 239 pp., 2011.

ACPD
14, 19357–19394, 2014

Kargas, G., Ntoulas, N., and Nektarios, P. A.: Soil texture and salinity effects on calibration of TDR300 dielectric moisture sensor, Soil Research, 51, 330–340, 2013.
Kirkman, G. A., Yang, W. X., and Meixner, F. X.: Biogenic nitric oxide emissions upscaling: an approach for Zimbabwe, Global Biogeochem. Cy., 15, 1005–1020, 2001.
Koeppen, W.: Grundriss der Klimakunde, Gruyter Verlag, Berlin/Leipzig, Germany, 388 pp., 1931.
Kurucz, R. L., Furenlid, I., Brault, J., and Testerman, L.: Solar Flux Atlas from 296 nm to 1300 nm, National Solar Observatory Atlas No. 1 Office of University publisher, Harvard University, Cambridge, 1984.
Lei, J. and Zhang, X. L.: Structural adjustment of oasis agriculture in Xinjiang, Chinese Journal of Population, Resources and Environment, 3, 29–33, 2005.
Leighton, P. A.: Photochemistry of Air Pollution, Academic Press, New York and London, 300 pp., 1961.
Leue, C., Wenig, M., Wagner, T., Platt, U., and Jähne, B.: Quantitative analysis of NO_x emissions from GOME satellite image sequences, J. Geophys. Res., 106, 5493–5505, 2001.
Ludwig, J., Meixner, F. X., Vogel, B., and Förstner, J.: Processes, influencing factors, and modelling of nitric oxide surface exchange – an overview, Biogeochemistry, 52, 225–257, 2001.
Mayer, J.-C., Bargsten, A., Rummel, U., Meixner, F. X., and Foken, T.: Distributed modified bowen ratio method for surface layer fluxes of reactive and non-reactive trace gases, Agr. Forest Meteorol., 151, 655–668, 2011.
Meixner, F. X. and Yang, W. X.: Biogenic emissions of nitric oxide and nitrous oxide from arid and semiarid land, in: Dryland Ecohydrology, edited by: D'Odorico, P. and Porporat, A., Springer, Dordrecht, the Netherlands, 233tt255, 2006, 233–255, 2006.
Morse, A., Tasumi, M., Allen, R. G., and Kramber, W. J.: Application of the SEBAL Methodology for Estimating Consumptive Use of Water and Streamflow Depletion in the Bear River Basin of Idaho through Remote Sensing, Final report submitted to The Raytheon Systems Company, Earth Observation System Data and Information System Project, Boise, USA, 107 pp., 2000.
Otter, L. B., Yang, W. X., Scholes, M. C., and Meixner, F. X.: Nitric oxide emissions from a southern African Savannah, J. Geophys. Res., 104, 18471–18485, 1999.
Perumal, K. and Bhaskaran, R.: Supervised classification performance of multispectral images, Journal of Computing, 2–2, 124–129, 2010.

ACPD
14, 19357–19394, 2014

Rothman, L. S., Jacquemart, D., Barbe, A., Chris Benner, D., Birk, M., Brown, L. R., Carleer, M. R., Chackerian Jr, C., Chance, K., Coudert, L. H., Dana, V., Devi, V. M., Flaud, J.-M., Gamache, R. R., Goldman, A., Hartmann, J.-H., Jucks, K. W., Maki, A. G., Mandin, J.-Y., Massie, S. T., Orphal, J., Perrin, A., Rinsland, C. P., Smith, M. A. H., Tennyson, J., Tolchenov, R. N., Toth, R. A., Vander Auwera, J., Varanasi, P., and Wagner, G.: The HITRAN 2004 molecular spectroscopic database, J. Quant. Spectrosc. Ra., 96, 139–204, 2005.

Rudolph, J. and Conrad, R.: Flux between soil and atmosphere, vertical concentration profiles in soil, and turnover of nitric oxide: 2. Experiments with naturally layered soil cores, J. Atmos. Chem., 23, 275–300, 1996.

Rudolph, J., Rothfuss, F., and Conrad, R.: Flux between soil and atmosphere, vertical concentration profiles in soil, and turnover of nitric oxide: 1. Measurements on a model soil core, J. Atmos. Chem., 23, 253–273, 1996.

Richter, A. and Burrows, J. P.: Tropospheric NO_2 from GOME Measurements, Adv. Space Res., 29, 1673–1683, 2002.

Simiu, E. and Scanlan, R. H.: Wind Effects on Structures: Fundamentals and Applications to Design, 3rd edn., John Wiley & Sons, New York, USA, 704 pp., 1996.

Sinreich, R., Frieß, U., Wagner, T., and Platt, U.: Multi axis differential optical absorption spectroscopy (MAX-DOAS) of gas and aerosol distributions, Faraday Discuss., 130, 153–164, doi:10.1039/b419274p, 2005.

Solomon, S., Schmeltekopf, A. L., and Sanders, R. W.: On the interpretation of zenith sky absorption measurements, J. Geophys. Res., 92, 8311–8319, 1987.

Turner, D. B.: Workbook of Atmospheric Dispersion Estimates, 2nd edn., Lewis publisher, London, 175 pp., 1994.

van Dijk, S. and Meixner, F. X.: Production and consumption of NO in forest and pasture soils from the amazon basin, Water Air Pollut.-Focus, 1, 119–130, 2001.

van Dijk, S. M., Gut, A., Kirkman, G. A., Meixner, F. X., Andreae, M. O., and Gomes, B. M.: Biogenic NO emissions from forest and pasture soils: relating laboratory studies to field measurements, J. Geophys. Res., 107, LBA 25-1–LBA 25-11, doi:10.1029/2001JD000358, 2002.

Vandaele, A. C. Hermans, C. Simon, P. C. Roozendael, M. Carleer, J. M., and Colin, R.: Fourier transform measurement of NO_2 absorption cross-section in the visible range at room temperature, J. Atmos. Chem., 25, 289–305, 1996.

ACPD
14, 19357–19394, 2014

Volkamer, R., Spietz, P., Burrows, J., and Platt, U.: High-resolution absorption cross-sections of glyoxal in the UV-vis and IR spectral ranges, J. Photoch. Photobio. A, 172, 35–46, 2005.

Wagner, T., Ibrahim, O., Shaiganfar, R., and Platt, U.: Mobile MAX-DOAS observations of tropospheric trace gases, Atmos. Meas. Tech., 3, 129–140, doi:10.5194/amt-3-129-2010, 2010.

Wagner, T., Beirle, S., Brauers, T., Deutschmann, T., Frieß, U., Hak, C., Halla, J. D., Heue, K. P., Junkermann, W., Li, X., Platt, U., and Pundt-Gruber, I.: Inversion of tropospheric profiles of aerosol extinction and HCHO and NO_2 mixing ratios from MAX-DOAS observations in Milano during the summer of 2003 and comparison with independent data sets, Atmos. Meas. Tech., 4, 2685–2715, doi:10.5194/amt-4-2685-2011, 2011.

Wittrock, F., Oetjen, H., Richter, A., Fietkau, S., Medeke, T., Rozanov, A., and Burrows, J. P.: MAX-DOAS measurements of atmospheric trace gases in Ny-Ålesund – Radiative transfer studies and their application, Atmos. Chem. Phys., 4, 955–966, doi:10.5194/acp-4-955-2004, 2004.

Yang, W. X. and Meixner, F. X.: Laboratory studies on the release of nitric oxide from subtropical grassland soils: the effect of soil temperature and moisture, in: Gaseous Nitrogen Emissions from Grasslands, Wallingford, England, 67–70, 1997.

Yu, J., Meixner, F. X., Sun, W., Liang, Z., Chen, Y., Mamtimin, B., Wang, G., and Sun, Z.: Biogenic nitric oxide emission from saline sodic soils in a semiarid region, northeastern China: a laboratory study, J. Geophys. Res., 113, 1–11, 2008.

Yu, J., Meixner, F. X., Sun, W., Mamtimin, B., Wang, G., Qi, X., Xia, C., and Xie, W.: Nitric oxide emissions from black soil, northeastern China: a laboratory study revealing significantly lower rates than hiterto reported, Soil Biol. Biochem., 42, 1784–1792, 2010a.

Yu, J., Meixner, F. X., Sun, W., Mamtimin, B., Xia, C., and Xie, W.: Biogenic nitric oxide emission of mountain soils sampled from different vertical landscape zones in the Changbai Mountains, Northeastern China, Environ. Sci. Technol., 44, 4122–4128, 2010b.

ACPD
14, 19357–19394, 2014

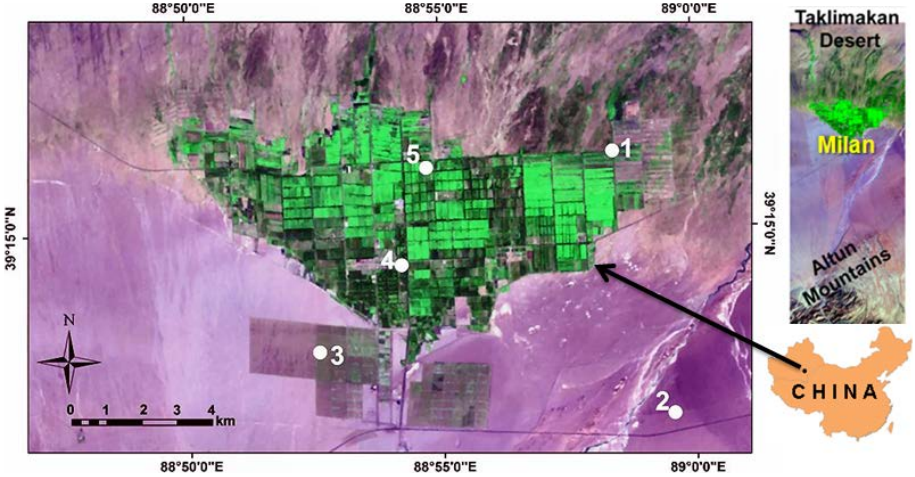

Figure 1. Satellite map (Landsat ETM+; 2011) of Milan oasis, Xinjiang, NW-China (The map has an area of 338 km^2). The white circles show the sites of in situ measurements: natural forest (1), desert (2), jujube (3), hotel/oasis station (4) and cotton field (5).

ACPD
14, 19357–19394, 2014

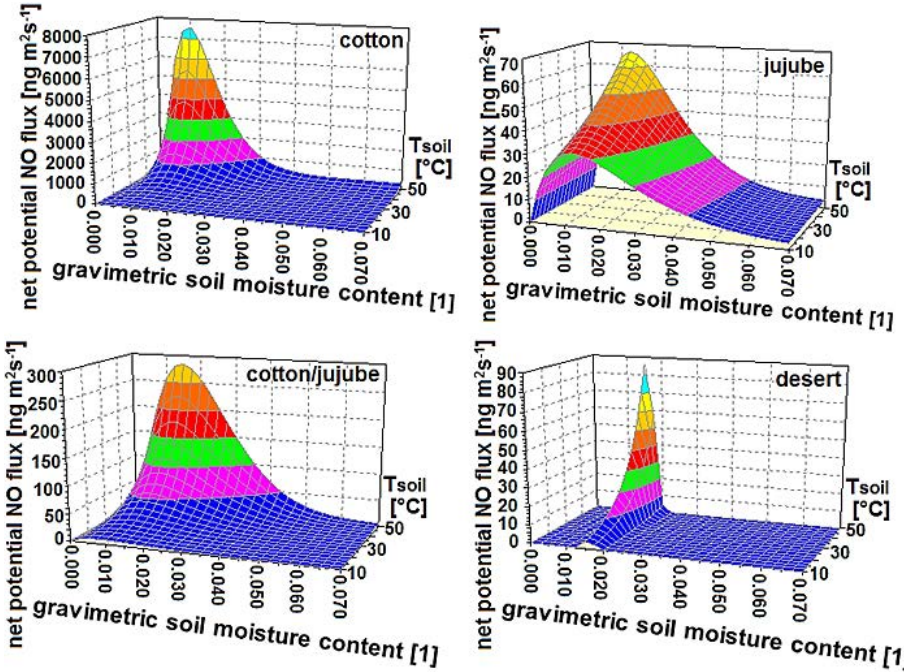

Figure 2. Net potential NO fluxes F_{NO} ($ng\,m^{-2}\,s^{-1}$; in terms of mass of nitric oxide) from soils of the four major land-cover types of Milan oasis as functions of soil temperature (°C) and dimensionless gravimetric soil moisture content.

ACPD
14, 19357–19394, 2014

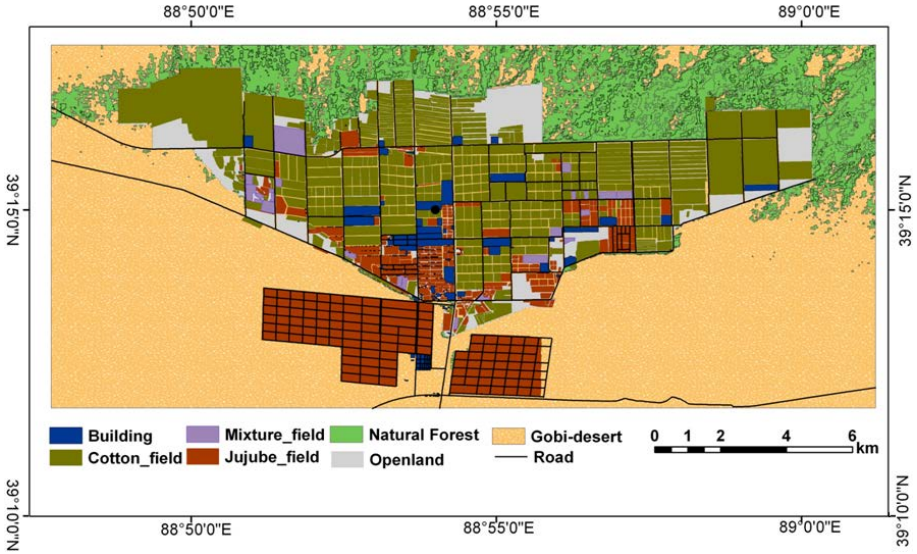

Figure 3. 2011 map of land-cover types of Milan oasis as derived from satellite images (Quickbird, Landsat ETM+, see Sect. 2.2.5).

ACPD
14, 19357–19394, 2014

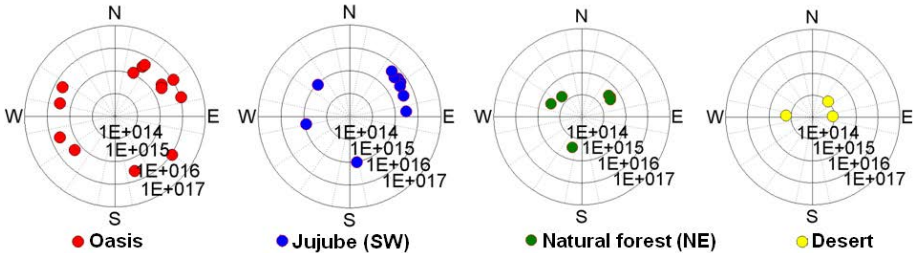

Figure 4. Results of MAX-DOAS measurements performed at sites oasis/hotel (4), Jujube (3), Natural forest (1), and Desert (2) of Milan oasis from 23 May to 26 June 2011 (see Fig. 1). Vertical NO_2 column densities (in molecules cm^{-2}; 20–30 min averages) are shown in relation to in situ measured wind direction at each location of MAX-DOAS measurements. The MAX-DOAS measurements were performed between 6:00 and 19:00 (local time). Note the radial logarithmic scale of VCD data.

ACPD
14, 19357–19394, 2014

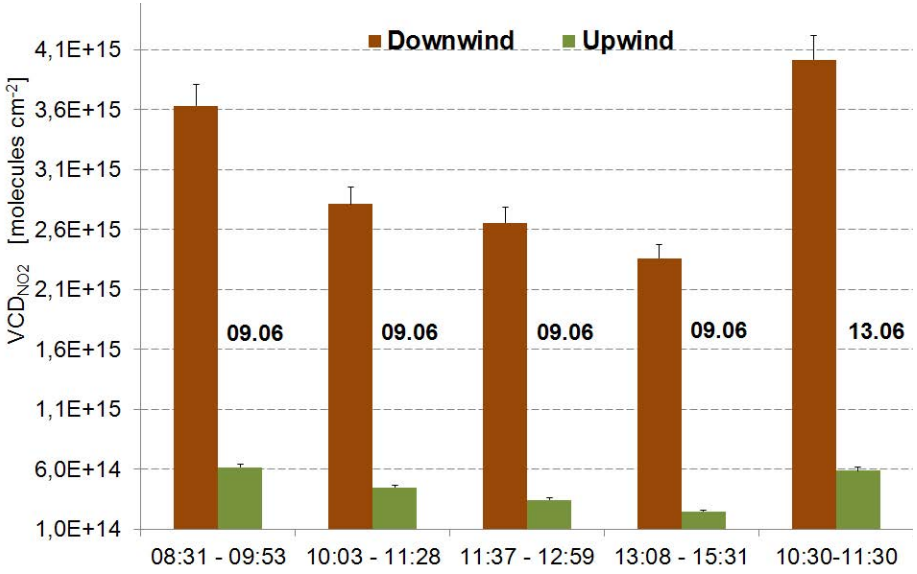

Figure 5. Results of NO_2-VCD measured simultaneously with two MAX-DOAS instruments upwind (natural forest, site (1)) and downwind (jujube field, site (3)) of Milan oasis on 09 and 13 June 2011.

ACPD
14, 19357–19394, 2014

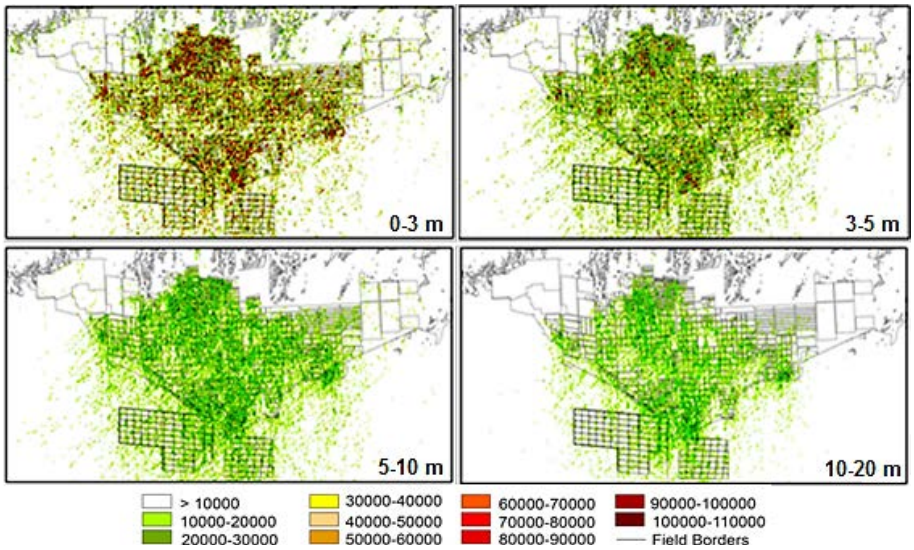

Figure 6. Results of NO concentrations (ng m^{-3}; in terms of mass of nitric oxide) calculated by the LASAT dispersion model for the first four vertical levels on 09 June 2011, 11:30 to 13:00 (local time).

ACPD
14, 19357–19394, 2014

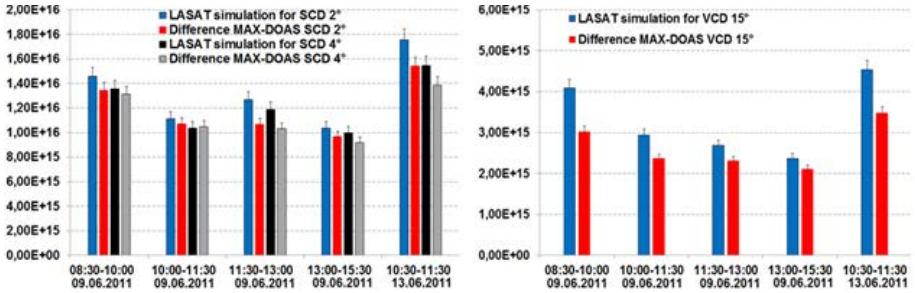

Figure 7. Simulated SCDs vs. SCDs measured by MAX-DOAS **(a)** and simulated VCDs vs. VCDs measured by MAX-DOAS **(b)** on 09 and 13 June 2011 at Milan oasis. SCDs have been measured and simulated for elevation angles of 2° and 4°, VCDs were measured at 15°.

ACPD
14, 19357–19394, 2014